

## **OBSERVATIONS OF L- AND C-BAND BACKSCATTER AND A SEMI-EMPIRICAL BACKSCATTERING MODEL APPROACH FROM A FOREST-SNOW-GROUND SYSTEM**

**A. N. Arslan**

Nokia Research Center  
Nokia Group  
P.O. Box 407, FIN-00045, Finland

**J. Pulliainen and M. Hallikainen**

Laboratory of Space Technology  
P.O. Box 3000, FIN-02015, HUT, Finland

**Abstract**—Observations of L- and C-band backscatter from snow cover are presented at all polarizations. Airborne passive-microwave data was collected in Northern Finland during EMAC'95 (European Multi-sensor Airborne Campaign-95). The measurements cover the 6.8–18.7 GHz frequency range with both vertical and horizontal polarizations. The empirical SAR data were acquired by EMISAR of Technical University of Denmark over the city of Oulu in Northern Finland during EMAC'95. Airborne measurements were conducted on 22–23 March, and on 2–3 May 1995. The land-use map of the test sites was obtained from the National Land Survey of Finland. This study combines the semi-empirical and empirical models that were developed. Applicability of the forest transmissivity formulas developed by using the different data sets of passive and active sensors is shown. Because of the effect of dry snow at C-band is more visible than at L-band. A C-band semi-empirical backscattering model is developed for the forest-snow-ground system.

### **1. INTRODUCTION**

In the field of microwave remote sensing, the physical phenomena governing the backscattering from the land-cover such as snow, forest, soil, etc., is very a complicated problem due to the complex behavior

of microwave interaction of the land-cover. To understand the problem better it necessitates simplification and practical applications such as mapping of snow and forest, weather forecast, water supply, flooding, forest damage, and etc. Microwave sensors such as radiometers and radars are often used for snow and forest studies in microwave remote sensing because of their usability in different weather conditions such as clouds, rain and lack of light. Active microwave sensors have proven to be a valuable tool in the microwave remote sensing of snow cover [1–12]. In forest applications, active microwave sensors are mainly used because they have better ground resolution than passive microwave sensors and the intensities of the microwave thermal emission from ground are close to those from the forest in most of the cases. Many studies have been conducted concerning the utilization of radar remote sensing for forest applications [13–18].

Because of the penetration capability of radar signal in land-cover, the use of synthetic aperture radar (SAR) data is a promising method for determination of large-scale snow and forest parameters such as snow density, snow water equivalent, snow wetness, stem volume, tree height, tree age, and forest floor type. Airborne SAR data and ground-based scatterometers are often used to make reference measurement for space-borne radars. A good spatial resolution and excellent localization of Airborne SAR data gives better understanding of the backscattering from land-cover, better theoretical, semi-empirical and empirical backscattering models and new research techniques.

In this paper, active microwave remote sensing of snow and forest is studied. The airborne backscattering coefficient data acquired by EMISAR (C- and L-band) of Technical University of Denmark in Northern Finland is analyzed. A statistical analysis for the backscattering coefficient and snow water equivalent was carried out for EMISAR data. The analysis covers three snow test sites (1,2 and 4) for both a dry snow situation on 22 March 1995 and snow-free situation on 2 May 1995. A semi-empirical backscattering model of forest canopy covered by snow, which is a function of the forest stem volume, and the snow water equivalent is developed.

## 2. DESCRIPTION OF DATA SET

### 2.1. Test Sites and Ground Truth Data

The EMAC'95 snow test sites are located along a straight line in northern Finland extending from the coast (near city of Oulu) to inland. The test sites are 9 km by 9 km squares and they consist of open areas (agricultural land) and forested areas (pine dominated forest). The analysis covers three snow test sites (1, 2 and 4). The

coordinates of the test sites along with the elevation above the sea level and the main land-cover category are shown in Table 1. The land-use map of the test sites was obtained from the National Land Survey of Finland. The spatial resolution of the map is 25 m by 25 m. Ground truth data was collected along the center-line of each test site by the Helsinki University of Technology and Finnish Environment Institute. The forest canopy data was provided by the Finnish Forest Research Institute.

Weather data was collected in test site 1 and test site 4. Since test site 1 and 2 are next to each other, weather data from test site 1 is valid also for test site 2. During EMISAR flights on 2–3 May no weather data was collected at the test sites, so we used weather data measured near the test sites by the Finnish Meteorological Institute. The daily air and snow surface temperatures for test sites 1 and 2, and 4 are shown in Table 2.

The ground-truth measurements include snow extent, snow depth, snow density profile, snow wetness profile, snow temperature, snow stratigraphy, snow grain size, land-use data (stem volume and land-use maps) and weather data [19]. Ground-truth data was collected on March 22, 1995 and on May 2, 1995. On March 22, the snowpack was dry, and its wetness was recorded to be less than 0.5% within the test

**Table 1.** Location (WGS84 coordinates), elevation above sea level and main land-cover type of the snow test sites.

Number	Start Coord. Elevation (m)	End Coord. Elevation (m)	Land-Cover Type
1	N64°47'31" E25°29'51 10	N64°50'38" E25°39'02" 17	Agricultural land
2	N64°50'38" E25°39'02" 17	N64°53'45" E25°48'14" 26	Pine forest
3	N65°12'44" E26°43'00 105	N65°15'46" E26°52'32" 118	Pine forest
4	N65°28'34" E27°30'57" 132	N65°31'31" E27°40'35" 190	Pine forest

**Table 2.** Daily maximum, average and minimum air and snow surface temperatures ( $^{\circ}\text{C}$ ) at test sites 1 and 2, and 4.

Test Site		22-23 March	2-3 May
1 and 2	Air	Max. 5.7 Av. -2.2 Min. -11.9	Max. 5.5 Av. 1.5 Min. -5.3
	Snow	Max. 0.0 Av. -2.1 Min. -6.1	
4	Air	Max. 4.6 Av. 0.4 Min. -14.7	
	Snow	Max. -0.4 Av. -2.2 Min. -3.9	

sites 1, 2 and 4. On May 2 the snowpack was wet and its wetness was recorded to vary from 0.5 to 1.8% within test sites 2 and 4. All snow had melted in test site 1 before May 2. Observed average values for snow and forest parameters in the test sites are given in Table 3. The density and wetness values are averages from the corresponding experimental profiles. The snow depth was measured every 100 meters, while snow density and snow wetness were recorded every 1000 meters. The snow water equivalent was calculated by multiplying snow density and snow depth.

**Table 3.** Average values of snow and forest parameters for test sites 1, 2 and 4.

Test Site	22 March 1995			2 May 1995		
	1	2	4	1	2	4
Stem Volume ( $\text{m}_3/\text{ha}$ )	0	58	56	0	58	56
Snow Depth (cm)	17	55	84	0	21	47
Snow Density ( $\text{g}/\text{cm}^3$ )	0.26	0.28	0.29	-	0.33	0.34
Snow Wetness (% vol)	0.35	0.31	0.36	-	1.08	1.15
Snow Water Equivalent (mm)	45	145	230	-	73	158

## 2.2. Microwave Data

Profiling passive-microwave data were acquired by the HUT (Helsinki University of Technology) radiometer HUTRAD [20] onboard the HUT Short Skyvan aircraft. On March 22, two measurement flights were conducted along the test lines in opposite directions. During the first flight, the radiometer system operated at 6.8 GHz and 18.7 GHz. While flying back, the 10.65-GHz channel was used, along with the 18.7 GHz. The receivers measured both vertically and horizontally polarized radiation. The incidence angle of the antenna beam was set to 50 degree off nadir. During the data collection, the nominal flight altitude was 300 meter and the nominal flight speed was 110 knots ( $\approx 59$  m/s), which resulted in footprint sizes in meters  $41 \times 93$ ,  $26 \times 70$ , and  $30 \times 77$  at 6.8, 10.65 and 18.7 GHz, respectively.

EMISAR is a dual frequency (L- and C-band) fully polarimetric (4 complex channels per frequency) Synthetic Aperture Radar (SAR) system developed for remote sensing applications. During 1994 and 1995 the SAR system was used to acquire polarimetric data for EMAC (European Multi-sensor Airborne Campaigns) arranged by ESA. EMISAR operates at L-band (1.25 GHz) and C-band (5.3 GHz) and measures at the two frequencies both the amplitude and relative phase of the backscattering coefficient for VV, HH, VH, and HV polarizations [21]. EMISAR data was collected on 22–23 March and 2–3 May 1995 for test sites 1,2 and 4, shown in Table 4. For both dates the data set includes two bands (L and C) in fully polarimetric mode. The nominal flight altitude is 12 km and the image swath is about 10 km. The incidence angle within the image varies from 40 to 60 degrees off nadir (mid-beam 50 to 53.5 degrees). The nominal resolution in slant range is 2 m. The intensity images of EMISAR were rectified into the Finnish National Coordinate System by using a digital elevation model. The geometric rectification was performed applying a polynomial rectification algorithm; however, no radiometric corrections due to topography were applied to the images. The final product of preprocessing is a rectified SAR image with a 5 m by 5 m pixel size. As a side product, a matrix containing the relative pixel sizes was also calculated.

## 3. SEMI-EMPIRICAL BACKSCATTERING MODEL

The total backscattering coefficient of the forested snow-covered ground is divided into two (incoherent) contributions that are given as follows,

$$\sigma^0 = \sigma_{can}^0 + t^2 \sigma_{floor}^0 \quad (1)$$

**Table 4.** EMISAR images for the snow test sites.

EMISAR data			
Date	Test Sites	Frequency (GHz)	Polarization
22 March 1995	1, 2, 4	1.25	VV, VH, HH, HV
23 March 1995	1, 2, 4	5.3	VV, VH, HH, HV
2 May 1995	1, 2, 4	1.25	VV, VH, HH, HV
3 May 1995	1, 2, 4	5.3	VV, VH, HH, HV

where

$$\begin{aligned} \sigma_{can}^0 &= \text{the backscattering coefficient from forest canopy,} \\ \sigma_{floor}^0 &= \text{the backscattering coefficient from ground floor,} \\ t^2 &= \text{the two way transmissivity of the forest canopy.} \end{aligned}$$

In case of ERS (European Remote Sensing Satellite) SAR observations (i.e., for C-band, VV-polarized observations at  $23^\circ$  angle of incidence), the average backscattering coefficient  $\sigma^0$  of forested land-cover can be approximately modeled ignoring trunk-ground and other multiple scattering mechanisms by [22, 23]

$$\begin{aligned} \sigma^0(V, \theta, m_{v,can}, \sigma_{ground}^0) &= \sigma_{can}^0(V, \theta, m_{v,can}) \\ &\quad + t^2(V, \theta, m_{v,can}) \cdot \sigma_{ground}^0 \\ &\equiv \sigma_{can}^0 + \sigma_{floor}^0 \end{aligned} \quad (2)$$

where  $\sigma_{ground}^0$  is the ground layer backscatter. The canopy backscattering contribution  $\sigma_{can}^0$  is equal to

$$\sigma_{can}^0(V, \theta, m_{v,can}) = \frac{\sigma_v(\theta, m_{v,can}) \cos(\theta)}{2\kappa_e(\theta, m_{v,can})} \cdot (1 - t^2(V, \theta, m_{v,can})) \quad (3)$$

and the two-way forest canopy transmissivity  $t^2$  is equal to

$$t^2(V, \theta, m_{v,can}) = \exp(-2\kappa_e(\theta, m_{v,can}) \cdot V / \cos(\theta)) \quad (4)$$

In (2)–(3),  $V$  is the total stem volume of forest (forest stand),  $\theta$  is the angle of incidence and  $m_{v,can}$ , is the effective vegetation (forest canopy) volumetric water content. The forest canopy extinction and volume backscattering coefficients ( $\kappa_e$  and  $\sigma_v$ , respectively) are

the parameters originally retrieved from scatterometer observations ( $\kappa_e \sim m_v$  and  $\sigma_v \sim m_v^2$ ).

The influence of parameters  $\kappa_e$ ,  $\sigma_v$ , and  $\sigma_{ground}^0$  in (2)–(3) can be reduced into two empirical coefficients [24]. The boreal forest backscattering model (2) can be rewritten based on inversion algorithm reference (training) data that must be available from the study region as

$$\begin{aligned}\sigma^0(V, \theta) &= 0.349 \cdot a \cos(\theta) \left( 1 - \exp \left( -1.36 \cdot 10^{-2} \frac{aV}{\cos(\theta)} \right) \right) \\ &\quad + b \exp \left( -1.36 \cdot 10^{-2} \frac{aV}{\cos(\theta)} \right) \\ &\equiv \sigma_{can}^0 + \sigma_{floor}^0\end{aligned}\quad (5)$$

where parameter  $a$  is related to the volumetric vegetation water content (in this study  $a$  is equal to 0.75 [24]) and parameter  $b \equiv \sigma_{ground}^0$ .

In this study, we also used an empirical boreal forest canopy transmissivity model which was developed on the basis of passive microwave measurements [20].

Airborne passive-microwave data was collected in Northern Finland during EMAC'95. The measurements cover the 6.8–18.7 GHz frequency range with both vertical and horizontal polarizations. On the basis of passive microwave measurements, an empirical forest transmissivity model is developed. The model is valid at vertical polarization, 50° incidence angle, and it accounts for microwave frequency and forest stem volume effects in the range of 6.8–94 GHz and 0–150 m<sup>3</sup>/ha, respectively.

The empirical boreal forest canopy transmissivity model predicts a decrease of forest canopy transmissivity with frequency and stem volume. The forest canopy transmissivity was calculated from brightness temperature measurements as a function of frequency  $f$  and stem volume  $V$ :

$$t(f, V) = \sqrt{\frac{T_B(f, V) - T_0}{T_B(f, 0) - T_0}} \quad (6)$$

where  $T_B(f, V)$  and  $T_B(f, 0)$  are brightness temperatures of forest and clear cut, respectively. The derivation of (2) is based on the assumption that snow air  $T_{air} \approx T_{snow}$ .

The forest canopy transmissivity at vertical polarization, 50° incidence angle, as function of frequency  $f$  [GHz] and forest-stem volume  $V$  [m<sup>3</sup>/ha] is given as follows [21],

$$t(f, V) = t(f, \mathbf{V}_{high}) [1 - t(f, \mathbf{V}_{high})] \cdot \exp(-0.035 \cdot V) \quad (7)$$

$t(f, \mathbf{V}_{high}) = 0.42 + (1 - 0.42) \cdot \exp(-0.028 \cdot f)$  that is frequency dependent transmissivity of a very dense forest, i.e. the saturation value of forest transmissivity at a certain frequency.

The backscattering coefficient from ground floor of the forest,  $\sigma_{floor}^0$ , is modeled empirically as follow [25, 26],

$$\sigma_{floor}^0(dB) = a \cdot swe + b, \quad (8)$$

where  $a$  and  $b$  are constant coefficients and  $swe$  is snow water equivalent of dry snow (mm). The coefficients were determined by the least square sum fitting of (8) to the measurement data. The values obtained for  $a$  and  $b$  are 0.0264 and  $-19.089$  respectively.

We examined in our previous studies [27, 28] radar backscatter from a half-space of wet snow and the effect of the size and shape of water inclusions on the backscattering coefficient. Wet snow is assumed to consist of dry snow (host) and liquid water (inclusions). As a future work, we examine radar backscatter from a half-space of dry snow using strong fluctuation theory and verify the empirical model presented in this paper.

#### 4. DATA ANALYSIS AND RESULTS

The backscattering coefficients for snow-covered and snow-free non-forested (open) areas were calculated as average values for sample plots of 25 m by 25 m along the test site center-line, where the snow ground truth measurements were conducted, using an interval of 100 meters. The center-line means that the same incidence is used for all samples. A statistical analysis is carried out between the backscattering coefficient and snow water equivalent for the chosen sample plots given in Table 5. The sample plots were chosen from homogeneous open areas. The sample plots from both ground data and the rectified images were checked. The agricultural open areas that do not have short vegetation, bushes, or mires are marked. The sample plots that were not clearly non-forested areas such as those containing bushes, short vegetation or mire are rejected. The analysis covers two situations (March and May), three snow test sites (1, 2 and 4) and all polarizations for L- and C-band.

Table 6 shows the results from the correlation analysis between EMISAR-derived backscattering coefficients, and ground truth parameters for 22 March 1995 and various test sites. The results indicate that the highest correlation with the backscattering coefficient is obtained for snow depth and snow water equivalent. The results show no correlation for the snow wetness.

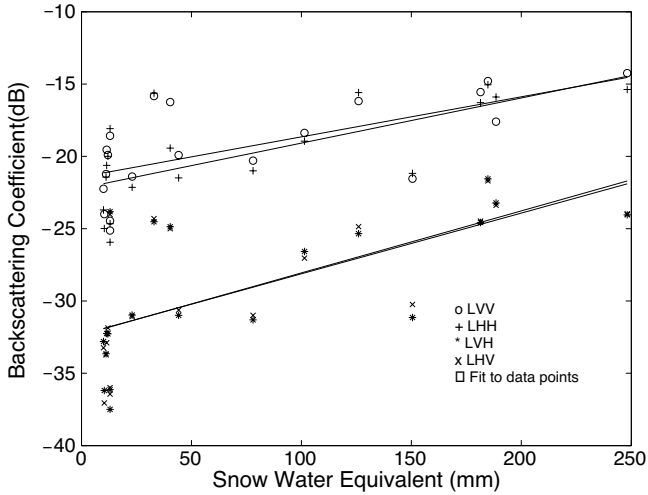


**Figure 1.** Correlation between backscattering and snow water equivalent at L-band in March under dry snow condition for the chosen sample plots given in Table 5. Solid lines represent regression lines fitted to the data in the least square sense.

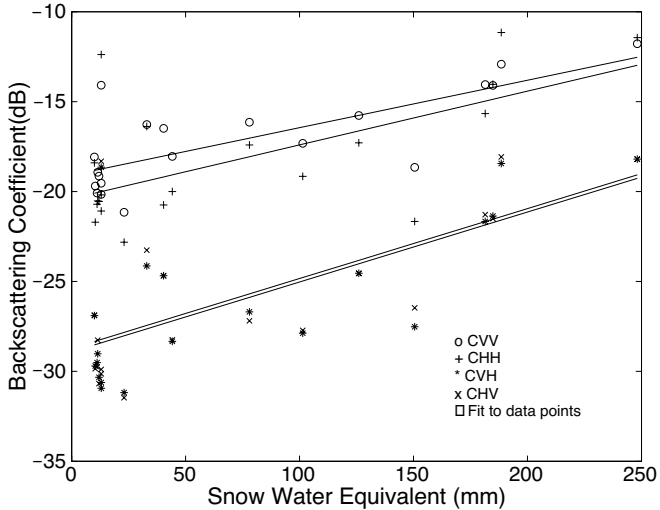


**Figure 2.** Correlation between backscattering and snow water equivalent at C-band in March under dry snow condition for the chosen sample plots given in Table 5. Solid lines represent regression lines fitted to the data in the least square sense.

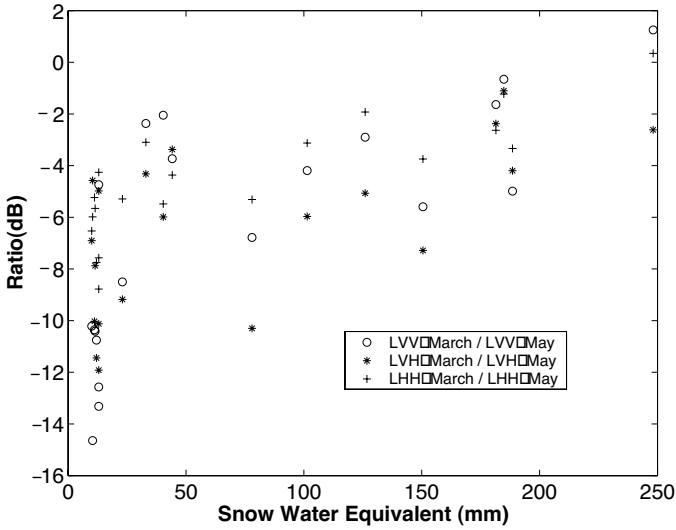


**Figure 3.** Comparison between observed backscattering coefficients in March under dry snow conditions and those in May under snow-free conditions at L-band.

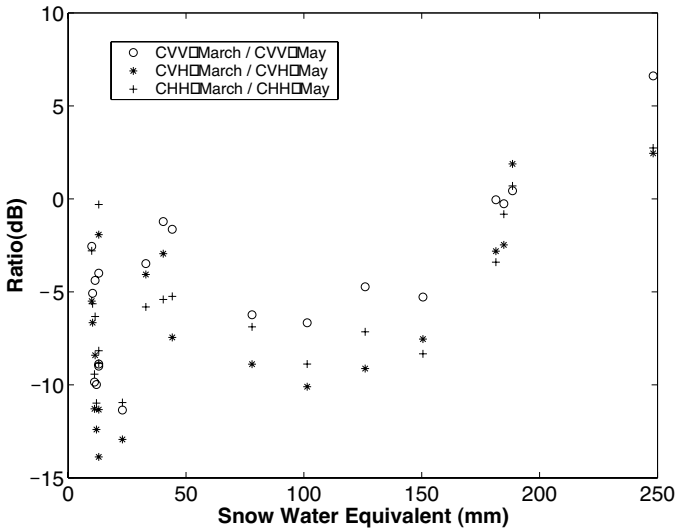


**Figure 4.** Comparison between observed backscattering coefficients in March under dry snow conditions and those in May under snow-free conditions at C-band.

**Table 5.** Snowpack parameters for selected sample plots in non-forested(open) test sites 1,2, and 4 on 22 March, 1995.

Test Site	Snow Density (gr/cm <sup>3</sup> )	Snow Depth (cm)	Snow Water Equivalent (mm)	Snow Wetness (%vol)
<b>Test Site 1</b>	0.256	9	23.04	0.23
	0.26	39	101.4	
	0.284	53	150.52	0.27
	0.26	5	13	
	0.3	4	12	0.25
	0.26	4	10.4	
	0.16	7	11.2	0.21
	0.26	5	13	
	0.269	15	40.35	0.27
	0.26	5	13	
	0.3	11	33	0.52
	0.26	17	44.2	
	0.2	5	10	0.5
	0.26	30	78	
	0.287	4	11.48	0.25
<b>Test Site 2</b>	0.324	56	181.44	0.16
	0.28	45	126	
	0.28	66	184.8	
<b>Test Site 4</b>	0.264	94	248.16	0.24
	0.29	65	188.5	

Figures 1 and 2 show the correlation in March under dry snow condition at L- and C-band, respectively. In spite of the small number of data points, the results suggest that there is a positive linear trend between the backscattering coefficient and snow water equivalent for both L- and C-band. When there is a little snow between 0–50 mm range of snow water equivalent the scattering is varying a lot. This may be explained due the strong effect of ground. When the snow water equivalent increases scattering becomes more linear. Figures 3 and 4 show backscattering coefficient ratios in dB between dry snow and snow free conditions at L-and C-band, respectively for VV, VH and HH polarizations. Spare distribution of scattering in the range of

**Table 6.** Computed correlation coefficients between the backscattering coefficients (dB) and ground data (snow depth, snow density, snow wetness, and snow water equivalent) for homogenous open areas (non-forested).

Correlation between ground data and backscattering coefficient for test sites 1, 2 and 4								
	22 March, EMISAR							
	CVV	CVH	CHV	CHH	LVV	LVH	LHV	LHH
Snow Depth (cm)	0.76	0.68	0.68	0.64	0.65	0.65	0.66	0.69
Snow Density (g / cm <sup>3</sup> )	0.37	0.29	0.34	0.20	0.52	0.53	0.56	0.58
Snow Wetness (% vol)	-0.01	0.03	0.07	0.13	-0.08	0.03	0.02	-0.07
Snow Water Equivalent (mm)	0.79	0.79	0.79	0.69	0.57	0.59	0.63	0.62

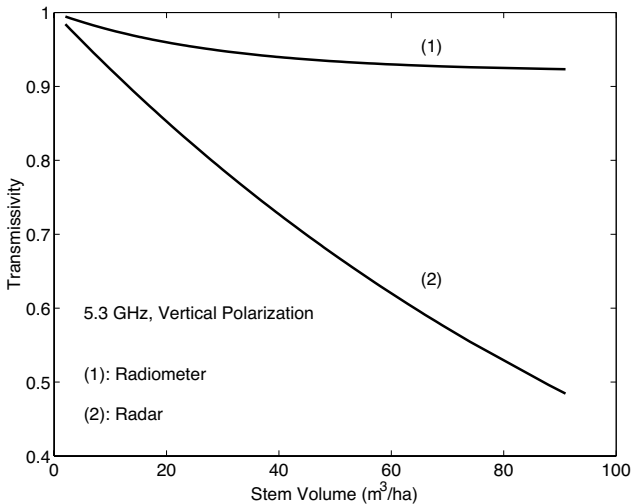


**Figure 5.** The forest transmissivity at vertical polarization, 50° incidence angle, as function forest-stem volume  $V$  [m<sup>3</sup>/ha] at 5.3 GHz.

0–50 mm of snow water equivalent is also noticed at both L- and C-band. At higher values of snow water equivalent, the effect of dry snow is more visible. The maximum changes of backscattering coefficient in dB are in the range of 7 dB at L-band and 11 dB at C-band when snow water equivalent changes from 78 mm to 248 mm.

By using (4) and (7), we calculated the forest canopy transmissivity depicted in Figure 5 respectively, at vertical polarization, 50°

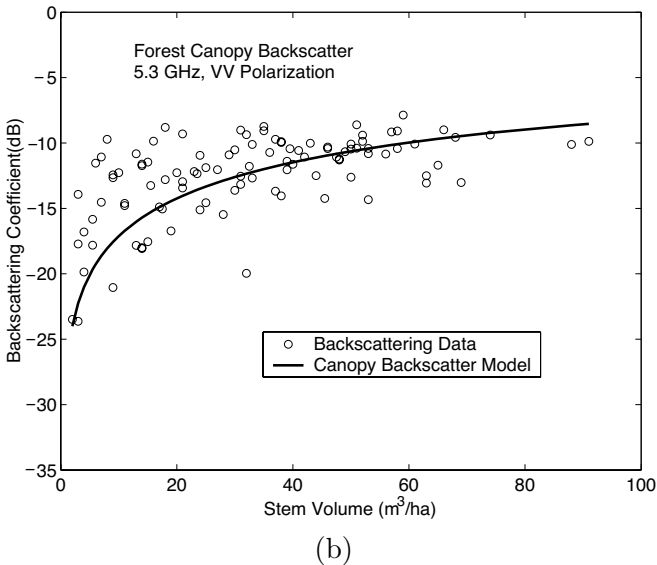
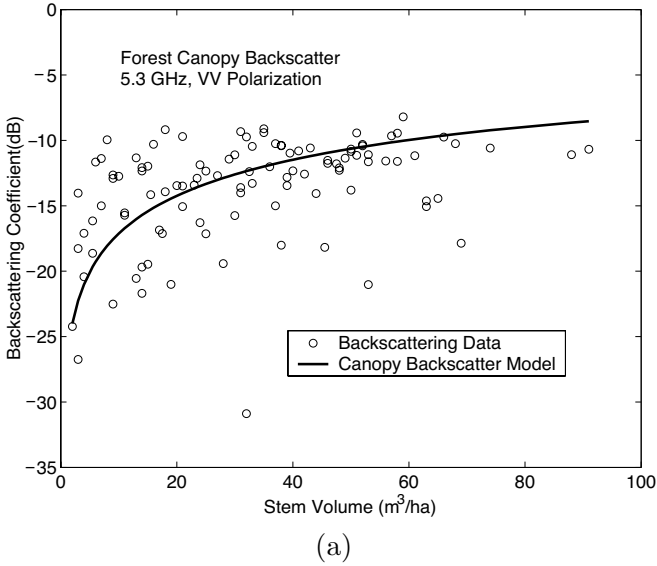


**Figure 6.** Canopy backscattering contribution  $\sigma_{can}^0$  at 5.3 GHz, VV polarization. Solid curve is the estimate according to Equation (3): (a)-the forest transmissivity model developed on the basis of passive microwave measurement (b)-the forest transmissivity model developed on the basis of radar data.

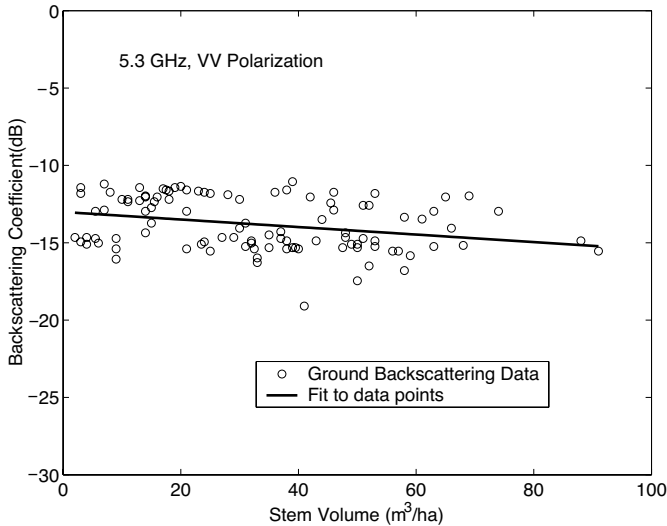


**Figure 7.** Ground backscattering contribution  $\sigma_{ground}^0$  at 5.3 GHz, VV polarization. Solid curve is the fitting curve to the data.

incidence angle, as function forest-stem volume  $V$  [m<sup>3</sup>/ha] at 5.3 GHz. As it is seen clearly in Figure 5 that the behavior of forest canopy the transmissivity models on basis radiometry and radar data are different. The reason could be that transmissivity model on basis radiometry [21] assumes that the scattering of the forest canopy is negligible. Forest canopy is assumed to be a pure attenuating layer. The formulation predicts a kind of effective transmissivity, not the real transmissivity of a layer that both scatters and absorbs radiation.

The forest canopy transmissivity (4) and (7) can be evaluated respectively by comparing the  $\sigma_{can}^0$  modeled by (3) with the data points shown in Figure 6. The canopy backscatter model shown in Figure 6a includes the forest transmissivity model developed on the basis of passive microwave measurement. The backscatter model on the basis of radar data shown in Figure 6b includes the forest canopy transmissivity model developed on the basis of radar data. The canopy backscatter model in Figure 6b gives better match with the data.

Figure 7 shows, the behavior of ground backscattering data versus stem volume. The backscattering is decreasing when stem volume increases as expected.

We have calculated the total backscattering coefficient by using forest canopy semi-empirical backscatter model and the empirical ground model.

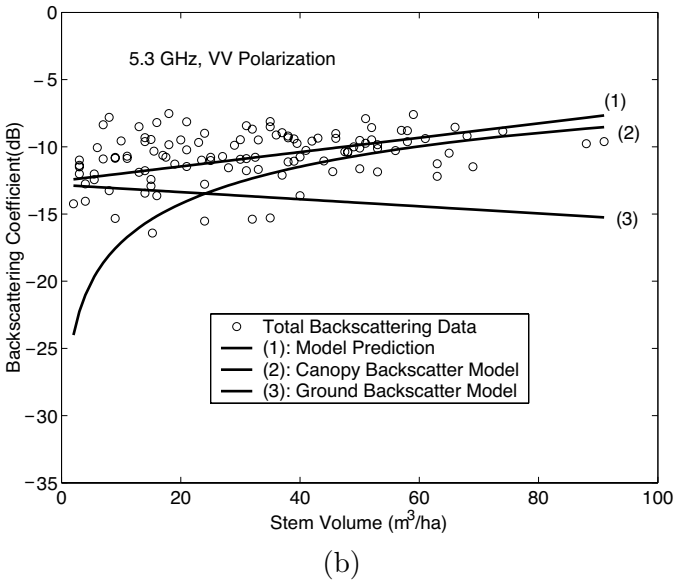
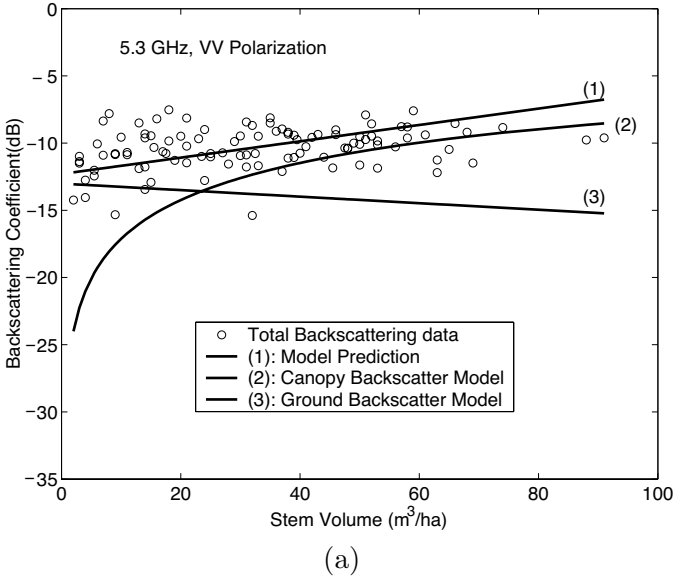


**Figure 8.** Backscattering contributions as a function of stem volume at 5.3GHz, VV polarization: (a)-the forest transmissivity model developed on the basis of passive microwave measurement (b)-the forest transmissivity model developed on the basis of radar data.

Figure 8 shows the total backscattering coefficients data, the total backscattering model and backscattering contributions from the forest canopy backscatter model and the ground floor as function of stem volume at 5.3 GHz, VV polarization, and  $50^\circ$  incidence angle.

## 5. CONCLUSIONS

We presented the observations of L- and C-band backscatter from snow cover at all polarizations. The results indicate that the highest correlation with the backscattering coefficient is obtained for snow depth and snow water equivalent. The results show no correlation for the snow wetness. At higher values of snow water equivalent, the effect of dry snow is more visible. The maximum changes of backscattering coefficient in dB are in the range of 7 dB at L-band and 11 dB at C-band when snow water equivalent changes from 78 mm to 248 mm. In spite of the small number of data points, the results suggest that there is a positive linear trend between the backscattering coefficient and snow water equivalent for both L- and C-band. Dry snow at C-band is more visible than at L-band. Of course, one should take into account the strong effect of ground at L- and C-band.

The semi-empirical backscattering model approach from a forest-snow-ground system is shown with combining the semi-empirical and empirical models developed on the different data sets of passive and active sensors. The results of the empirical backscattering modeling of snow and the semi-empirical backscattering modeling of forest canopy covered by snow presented in this paper are important due to the following reasons: (a) backscattering modeling of snow using SAR data is still under study by many researchers and different results have been published in the literature, (b) because of the availability of empirical data (even though it is very limited) on forest-snow-ground system, the developed semi-empirical backscattering model with applicability of the forest transmissivity formulas developed by using the different data sets of passive and active sensors may give a better understanding of forest-snow-ground system for future studies.

One should keep in mind that the formulas for the forest canopy transmissivities used in this study are given in the conditions and the some approximations where the measurements have been carried out.

## REFERENCES

1. Shi, J. and J. Dozier, "Estimation of snow water equivalence using SIR-C/X-SAR, Part I: Inferring snow density and subsurface

- properties,” *IEEE Trans. Geosci. Remote Sensing*, Vol. 38, No. 6, 2465–2474, 2000.
2. Shi, J. and J. Dozier, “Estimation of snow water equivalence using SIR-C/X-SAR, Part II: Inferring snow depth and particle size,” *IEEE Trans. Geosci. Remote Sensing*, Vol. 38, No. 6, 2475–2488, 2000.
  3. Kendra, J. R., K. Sarabandi, and F. T. Ulaby, “Radar measurements of snow: experiment and analysis,” *IEEE Trans. Geosci. Remote Sensing*, Vol. 36, No. 4, 864–879, 1998.
  4. Bernier, M. and J. P. Fortin, “The potential of time series of C-band SAR data to monitor dry and shallow snow cover,” *IEEE Trans. Geosci. Remote Sensing*, Vol. 36, No. 1, 226–243, 1998.
  5. Strozzi, T., A. Wiesmann, and C. Mätzler, “Active microwave signatures of snow covers at 5.3 and 35 GHz,” *Radio Science*, Vol. 32, No. 2, 479–495, 1997.
  6. Koskinen, J., J. Pulliainen, and M. Hallikainen, “The use of ERS-1 SAR data in snow melt monitoring,” *IEEE Trans. Geosci. Remote Sensing*, Vol. 35, No. 3, 601–610, 1997.
  7. Shi, J. and J. Dozier, “Estimation of snow water equivalence using SIR-C/X-SAR,” *Proceedings of IGARSS’96*, Vol. 4, 2002–2004, 1996.
  8. Shi, J. and J. Dozier, “Inferring snow wetness using C-band data from SIR-C’s polarimetric synthetic aperture radar,” *IEEE Trans. Geosci. Remote Sensing*, Vol. 33, No. 4, 905–914, 1995.
  9. Rott, H. and T. Nagler, “Capabilities of ERS1-SAR for snow and glacier monitoring in alpine region,” *Proceedings of the Second ERS-1 Symposium*, 965–970, Eur. Space Res. and Technol. Cent., 1993.
  10. Mätzler, C. and E. Schanda, “Snow mapping with active microwave sensors,” *International Journal of Remote Sensing*, Vol. 15, No. 2, 409–422, 1983.
  11. Stiles, W. H. and F. T. Ulaby, “The active and passive microwave response to snow parameters, 1, wetness,” *J. Geophys. Res.*, Vol. 85, 1037–1044, 1980.
  12. Ulaby, F. T. and W. H. Stiles, “The active and passive microwave response to snow parameters, 1, water equivalent of dry snow,” *J. Geophys. Res.*, Vol. 85, 1045–1049, 1980.
  13. Dobson, M. C., F. T. Ulaby, T. Le Toan, A. Beaudoin, E. S. Kasischke, and N. Christensen, “Dependence of radar backscatter on coniferous biomass,” *IEEE Trans. Geosci. Remote Sensing*, Vol. 30, No. 2, 412–415, 1992.

14. Durden, S. L., J. J. Van Zyl, and H. A. Zebker, "Modeling and observation of the radar polarization signature of forested areas," *IEEE Trans. Geosci. Remote Sensing*, Vol. 27, No. 3, 290–301, 1989.
15. Le Toan, T., A. Beaudoin, J. Riom, and D. Guyon, "Relating forest biomass to SAR data," *IEEE Trans. Geosci. Remote Sensing*, Vol. 30, No. 2, 403–411, 1992.
16. Ulaby, F. T., K. Sarabandi, K. McDonald, M. Whitt, and M. C. Dobson, "Michigan microwave scattering model," *Int. J. Remote Sensing*, Vol. 11, No. 7, 1223–1253, 1990.
17. Pulliainen, J., "Investigation on the backscattering properties of finnish boreal forests at C- and X-band: Semi-empirical modeling approach," Doctor of Technology Thesis, Report 19, 119, Laboratory of Space Technology, Helsinki University of Technology, Espoo, 1994.
18. Pulliainen, J., K. Heiska, J. Hyypä, and M. Hallikainen, "Backscattering properties of boreal forests at C- and X-band," *IEEE Trans. Geosci. Remote Sensing*, Vol. 32, No. 5, 1041–1050, 1994.
19. Hallikainen, M., J. Koskinen, J. Praks, A. N. Arslan, H. Alasalmi, and P. Makkonen, "Mapping of snow with airborne microwave sensors in EMAC'95," *Proc. EMAC Final Workshop*, 143–153, ESA-ESTEC, 1997.
20. Kruopis, N., J. Praks, A. N. Arslan, H. Alasalmi, J. Koskinen, and M. Hallikainen, "Passive microwave measurements of snow-covered forest areas in EMAC'95," *IEEE Trans. Geosci. Remote Sensing*, Vol. 37, 2699–2705, November 1999.
21. Christensen, E. L., N. Skou, J. Dall, K. W. Woelders, J. H. Jorgensen, J. Granholm, and S. N. Madsen, "MISAR: An absolutely calibrated polarimetric L- and C-band SAR," *IEEE Trans. Geosci. Remote Sensing*, Vol. 36, No. 6, 1852–1865, 1998.
22. Pulliainen, J., L. Kurvonen, and M. Hallikainen, "Multi-temporal behavior of L- and C-band SAR observations of boreal forest," *IEEE Trans. Geosci. Remote Sensing*, Vol. 37, 927–937, 1999.
23. Pulliainen, J., P. Mikkilä, and M. Hallikainen, "Seasonal dynamics of C-band backscatter of boreal forests with applications to biomass and soil moisture estimation," *IEEE Trans. Geosci. Remote Sensing*, Vol. 34, 758–770, May 1996.
24. Pulliainen, J., M. Engdahl, and M. Hallikainen, "Feasibility of multi-temporal interferometric SAR data for stand-level estimation of boreal forest stem volume," *Remote Sensing of Environment*, Vol. 85, 397–409, 2003.

25. Arslan, A. N., J. Koskinen, J. Praks, H. Alasalmi, N. Kruopis, and M. Hallikainen, "Retrieving snow water equivalence on C- and L-band SAR data for dry snow," *Proceedings of IGARSS'98*, Vol. 4, 1870–1872, 1998.
26. Arslan, A. N., J. Praks, J. Koskinen, and M. Hallikainen, "An empirical model for retrieving water equivalent of dry snow from C-band SAR data," *Proceedings of IGARSS'99*, Vol. 3, 1789–1791, 1999.
27. Arslan, A. N., H. Wang, J. Pulliainen, and M. Hallikainen, "Effective permittivity of wet snow using strong fluctuation theory," *Journal of Electromagnetic Waves and Applications*, Vol. 15, 53–55, 2001.
28. Arslan, A. N., H. Wang, J. Pulliainen, and M. Hallikainen, "Scattering from wet snow by applying strong fluctuation theory," *Journal of Electromagnetic Waves and Applications*, Vol. 17, 1009–1024, 2003.